ERC (2020) 34
Doi: 10. 19743/j.cnki.0891-4176. 202004007
Citation: MA Xingyu, WANG Lanmin, WANG Qian, WANG Ping, ZHONG Xiumei, PU Xiaowu, LIU Fuqiang, XU Xiaowei. Flow Characteristics of Large-Scale Liquefaction-Slip of the Loess Strata in Shibei Tableland, Guyuan City, Induced by the 1920 Haiyuan $M8\frac{1}{2}$ Earthquake [J]. *Earthquake Research in China*, 2020, 34(4): 469-481.

Flow Characteristics of Large-Scale Liquefaction-Slip of the Loess Strata in Shibei Tableland, Guyuan City, Induced by the 1920 Haiyuan $M8\frac{1}{2}$ Earthquake

MA Xingyu[1, 2], WANG Lanmin[1, 2], WANG Qian[1, 2)*], WANG Ping[1, 2], ZHONG Xiumei[1, 2], PU Xiaowu[1, 2], LIU Fuqiang[1, 3] and XU Xiaowei[1, 2]

1) Key Laboratory of Loess Earthquake Engineering, China Earthquake Administration, Lanzhou 730000, China
2) Lanzhou Institute of Seismology, China Earthquake Administration, Lanzhou 730000, China
3) Department of Civil Engineering and Mechanics, Lanzhou University, Lanzhou 730000, China

Based on the dynamic triaxial liquefaction test of the loess samples which are taken from Shibei tableland, Guyuan City, Ningxia, China, the characteristics of dynamic strain, dynamic stress and pore water pressure are studied under cyclic loading. Triaxial shear test is conducted immediately after the sample reaches liquefaction point. During the test, the property of the liquefied soil is analyzed through fluid mechanics method, whereby the fluidity of the liquefied soil is represented by apparent viscosity. The results show that the fluidity of liquefied loess changes from "shear thickening" to "shear thinning" as the shear force continues, and the fluidity of liquefied loess is closely related to its structure. In addition, in the process of forming a new stable state, the apparent viscosity and deviant stress change with axial strain in a similar approach. When the sample reaches its stable state, it meanwhile shows a relatively stable apparent viscosity. According to the fluid mechanics and the law of conservation of energy, the slip distance of the liquefied soil is estimated, and the results are in good agreement with the field investigation results.

Key words: Saturated loess; Hydrodynamics; Liquefaction; Apparent viscosity

INTRODUCTION

In recent years, large-scale liquefaction and sliding disasters of soil mass caused by

[1] Received on July 6th, 2020; revised on September 14th, 2020. This project is sponsored by the National Natural Science Foundation of China (U1939209, 51778590) and the Spark Program (XH20057).
* Corresponding author.

earthquakes have occurred frequently, raising extensive attention in a global scale. Numerous strong earthquakes, such as the 1920 Haiyuan $M8\frac{1}{2}$ earthquake (Bai Mingxue et al., 1990), the 1995 Osaka-Kobe M_S7.2 earthquake (Du Xiuli et al., 2018), the 2011 offshore earthquake in Northeast Japan (Huang Yu et al., 2013) and the 2018 Palu M_S7.5 earthquake in Indonesia (Watkinsonim H. R., 2019) have caused large-scale soil liquefaction and sliding disasters, resulting in a large number of casualties and property losses. Chen Wenhua (2001) qualitatively revealed the mechanism of liquefaction flow deformation through a large number of liquefaction flow phenomena, and proposed six flow slide models to explain part of the large deformation disasters induced by earthquake liquefaction. Liu Fang et al. (2013) analyzed the key factors which affect seismic liquefaction deformation measurement through data statistics. Hu Zhonghua et al. (2016), Chen Yumin et al. (2009) and Liu Hanlong et al. (2009) studied the mechanical properties and deformation characteristics of saturated sand after liquefaction by the fluid mechanics method. Zhuang Haiyang et al. (2016) analyzed the influence law and mechanism of rubber film effect, effective confining pressure, cyclic loading amplitude and initial static shear stress on large deformation characteristics of Nanjing fine sand liquefaction flow by conducting cyclic torsional shear test on saturated fine sand. Wei Xing et al. (2019) used particle flow software to simulate the cyclic shear test of saturated sand without drainage process, studied the influence of different factors on liquefaction, and further analyzed the basic features of macroscopic deformation of saturated sand after liquefaction. Zhou Zhenglong et al. (2017) studied the effect of initial shear stress on the characteristics of soil liquefaction and large deformation by cyclic torsional shear test.

The aforementioned investigations are mainly carried out on saturated sandy soil and silty soil. However, global seismic damage cases and laboratory experiments have proved that saturated loess and even loess with high water content have significant liquefaction potential; moreover, liquefaction can occur under a certain earthquake intensity, leading to large-scale liquefaction slip disaster of loess. Worldwide scholars have conducted abundant research on the liquefaction of saturated loess. Prakash S. et al. (1982) first proposed the phenomenon and its influence of loess liquefaction. Puri V.K. (1984) found that cyclic loading on saturated loess samples would cause an increase in pore water pressure, while the increase in soil plasticity would inhibit the increase in pore pressure, and finally proposed the occurrence condition of liquefaction flow failure for saturated loess. Ishihara K. et al. (1990) considered that the flow sliding phenomenon in Tajikistan of the former Soviet Union was caused by seismic liquefaction of loess. Deng Longsheng et al. (2012) suggested that residual strain could be used to describe the degree of loess liquefaction, with the support of triaxial test results. Wang Lanmin et al. (2000, 2013) detailed the change of pore water pressure in the liquefaction process of saturated loess and the criterion of loess liquefaction by using soil dynamics method through field survey and laboratory test. She Yuexin et al. (2002) studied the growth principle of pore pressure and the mechanism of loess liquefaction on a micro level through indoor dynamic triaxial test. Yang Zhenmao et al. (2004) conducted the consolidated undrained triaxial test under stress control, studied the steady state strength characteristic of the saturated loess as well as the over-consolidated influence on its undrained traits, and analyzed the similarities and differences of static liquefaction characteristics between loess and sand contrastively. Finally, they pointed out the conditions of saturated loess flow failure and the method of judging whether the saturated

loess can produce liquefaction flow slip by steady state strength. Deng Jin et al. (2013) studied the changes of soil microstructure in the process of loess liquefaction. Furthermore, studies on the liquefaction flow slide disaster of loess strata are briefly summarized as follows.Based on field investigations and laboratory test results of a large range of low-angle flow slides in Shibei tableland, Guyuan. Bai Mingxue et al. (1990) proposed that the flow slides were caused by seismic liquefaction and upwelling in the sand-bearing loess section of Malan loess in which the pushed the soil on both sides are pushed. Through dynamic triaxial test, Wang Qian et al. (2014) studied the liquefaction characteristics of loess in Shibei tableland and analyzed the loess liquefaction mechanism of the Haiyuan earthquake. Zhang Xiaochao et al. (2018) carried out an experimental investigation on the steady-state deformation characteristics of saturated loess with the support of a large ring shear apparatus, and discussed the influence of consolidation pressure, saturation, shear rate and other factors on the steady-state strength of loess. Wang Lanmin (2020) studied the conditions, kinematics and dynamics characteristics of large-scale liquefaction flow slides in loess strata through field investigation, laboratory test and numerical simulation analysis, discussed the flow slide mechanism, and built a prediction model of the distance and influencing range of the flow slides.

In summary, although the liquefaction characteristics and mechanism of saturated loess have been studied in a global scale, the main objects are mainly sandy soil and silty soil. On the basis of previous studies, this study conducts field investigation of the loess liquefaction flow slides in Shibei tableland generated by the 1920 Haiyuan earthquake, and selects exploration well samples from the loess site at the back edge of the flow slide area, and further completes the dynamic triaxial liquefaction test of the saturated undisturbed loess and triaxial shear test of the soil after liquefaction. The seismic liquefaction mechanism and characteristics of loess in Shibei tableland are studied and the flow characteristics of loess after liquefaction are studied using the fluid mechanics method. The results of this study are valuable for deepening our understanding of the forming mechanism of large-scale flow slides induced by loess liquefaction as well as providing a reference for the prevention of liquefaction flow slides in loess area.

1 MATERIALS AND METHODS

1.1 Sample and Instrument

In order to study the dynamic response of the sandy loess in the Haiyuan earthquake and its movement after liquefaction, we conducted a field survey in October 2019 in the flow slide area of the Loess Plateau. The Shibei tableland, located in the mountainous area of Southern Ningxia Hui Autonomous Region, is relatively sparsely populated. The Haiyuan earthquake occurred 100 years ago. During the long period, rainfall, slope erosion, human activities and other external disturbances on the flow slide area are inevitable. However, these disturbances affect mainly on topsoil. The local area is characterized by arid climate with scarce precipitation; thus, there is no runoff on the surface and the strata are relatively stable. The sampling site is located in the non-sliding loess strata at the rear edge, and the sampling depth is 15 m. During the sampling stage, 1.0–1.5 m of artificial excavation is made at the rear edge of the original landslide body. The cubic soil blocks which are 100

mm in length, 100 mm in width and 200 mm in height are collected and sealed on site and then transported to the laboratory for testing. Therefore, the soil samples are less subject to external interference factors, and its physical parameters change slightly compared with the soil 100 years ago. The sampling location and environment are shown in Fig.1 and Fig.2. The physical properties of soil samples are shown in Fig.3 and Table 1.

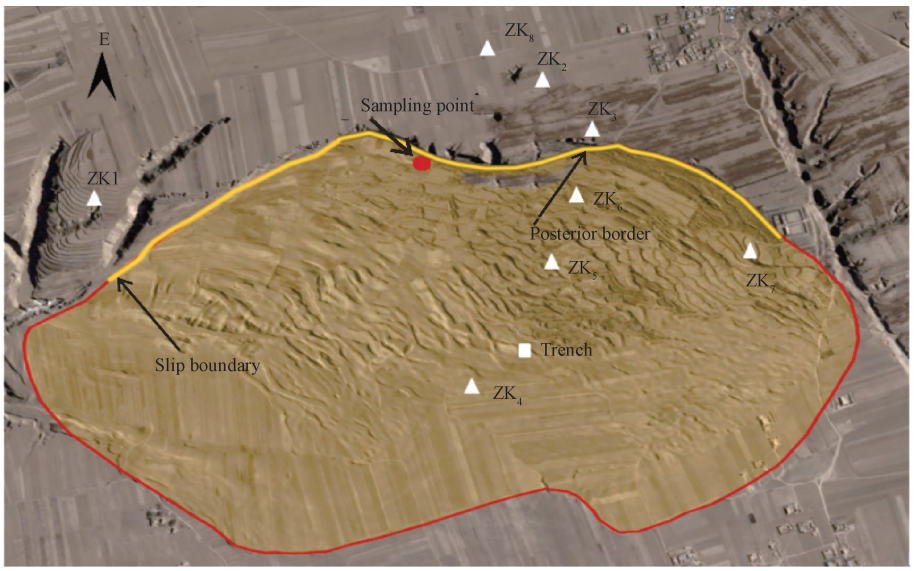

Figure 1 South flow slide boundary, sampling points and borehole layout (Wang Lanmin et al. 2020)

Figure 2 Sampling points of dynamic triaxial specimen

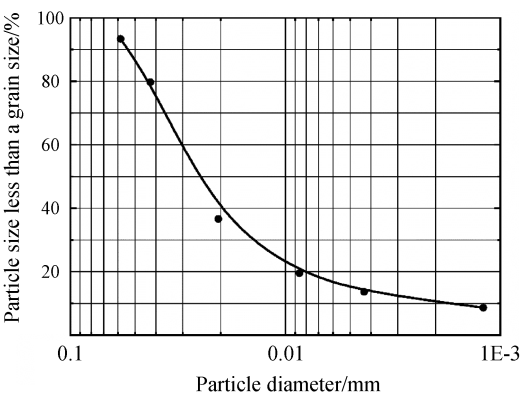

Figure 3 Grading curve of soil sample

Table 1 Physical property indexes of soil samples

Sample number	Sampling horizon	Sampling depth/m	Initial void ratio	Natural water content /%	Plasticity index
sby-1		15	0.74	5.8	7.0
sby-2	Sandy clay	15	0.62	5.6	7.4
sby-3		15	0.70	5.0	8.3

The laboratorial dynamic and static triaxial test are conducted on the WF-12440 model dynamic triaxial-hollow cylinder torsional shear test system in the Key Laboratory of Loess Seismic Engineering, China Earthquake Administration. The system is equipped with a back pressure saturation system, which can effectively increase saturation by applying back pressure step by step on the sample, thus ensuring the accuracy of liquefaction test.

1.2 Test Methods

The on-site soil samples are uniformly cut into cylindrical samples with a diameter of 50 mm× 100 mm. The samples are saturated by the back pressure saturation method. The saturability of the samples is determined by detecting the pore water pressure coefficient *b*-value. When the *b*-value reaches 0.95, the sample is consolidated. In order to reduce the deformation of the sample in the process of static pressure, the consolidation ratio $K_c = 1$ is selected, and the axial pressure and confining pressure are both 100 kPa. When the consolidation deformation is less than 0.0005 mm/min, the sample consolidation is considered stable. The consolidated and stabilized samples are subjected to cyclic shear under constant amplitude sinusoidal loads of different amplitudes. Considering the fact that for an earthquake, the higher acceleration, the longer duration time, and the lower frequency will produce more severe destruction. The test adopts the dynamic load with a frequency of 1 Hz. The liquefaction failure criteria of the sample is set as axial dynamic strain $\geqslant 3\%$ and pore water pressure ratio $U_d/\sigma'_0 \geqslant 0.2$ (Wang Lanmin et al., 2000). The dynamic stress, dynamic strain and dynamic pore water pressure are recorded during the test. Triaxial shear test is carried out immediately after the sample reaches liquefaction. The confining pressures of different samples are 140 kPa, 200 kPa and 250 kPa respectively and the shear rate is 0.4 mm/min.

2 RESULTS AND ANALYSIS

2.1 Results

According to the dynamic triaxial liquefaction test results, the dynamic stress-strain and dynamic pore water pressure changes and dynamic stress-strain hysteresis curves of saturated loess are drawn, as shown in Fig.4. It can be seen from Fig.4(a) that in the early stage of cyclic loading, the dynamic stress and strain change clighly, and the slope of the long-axis of hysteresis loop is large. At this time, the pore water pressure response is weak and only increases slowly. In addition, the soil structure is basically stable because of no residual deformation or small residual deformation. With the increase of vibration times, the dynamic stress decreases obviously, the dynamic residual strain increases rapidly, and the slope of the long-axis of the hysteretic curve decreases. At this time, the growth rate of pore

water pressure in soil is accelerating, and the effective stress is decreasing continuously. Finally, due to the decrease of effective stress, the strength of loess structure decreases continuously, exhibiting the characteristics of "cyclic activity" consequently. According to Fig.4(b), at the beginning of cyclic loading, the dynamic strain of saturated loess increases slowly and is mainly elastic strain. However, with the increase of vibration number, the growth of dynamic strain gradually accelerates. When the dynamic strain reaches about 2%, the area of hysteresis loop and the residual strain begin to increase rapidly, indicating that the structural strength of loess is weakening, and the ability of resisting deformation becomes worse.

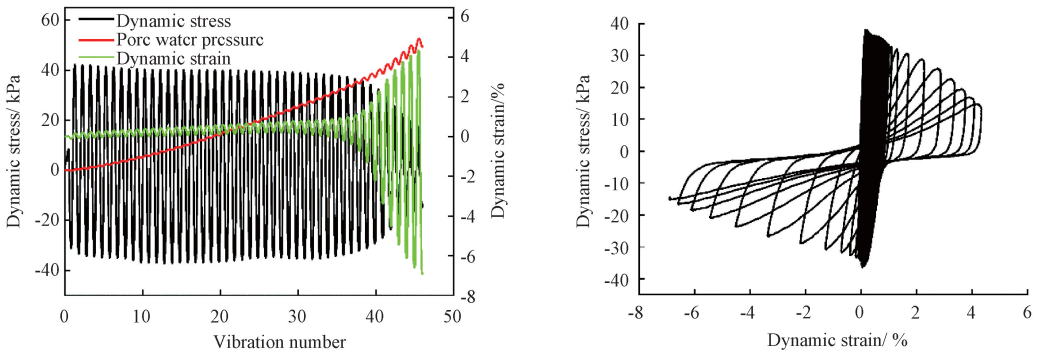

Figure 4 Dynamic triaxial test results

(a) Relationship between dynamic stress, dynamic strain, pore water pressure and number of vibration, (b) Curves of dynamic stress versus strain

2.2 *Flow Characteristics of Loess after Liquefaction*

Historical earthquake damage cases and indoor model test results in loess area show that (Bai Mingxue et al., 1990; Xu Shunhua et al., 2013; Wang Lanmin et al., 2015) saturated loess has a certain fluidity after liquefaction; thus, the loess mass can be regarded as fluid for simpler calculation. According to the principle of hydrodynamics, the viscosity of saturated loess in different time periods is analyzed. In order to study the process and formation mechanism of liquefaction and fluidization of saturated loess, we mainly rely on the results of triaxial shear test; moreover, the fluidity of saturated loess after liquefaction is characterized by calculating the apparent viscosity. As a result, the lower the apparent viscosity is, the better the fluidity is. The apparent viscosity is calculated by Equa.(1):

$$\eta(t) = \frac{\tau_a(t)}{\gamma_{\dot{a}}(t)} \tag{1}$$

In the equation, $\tau_a(t)$ and $\gamma_{\dot{a}}(t)$ are the shear stress and shear strain rate corresponding to the time; $\eta(t)$ is the apparent viscosity; $\gamma_{\dot{a}}(t)$ is calculated by Equa.(2).

$$\gamma_{\dot{a}}(t) = \frac{1}{2}\left(\frac{\gamma_{i+1} - \gamma_i}{t_{i+1} - t_i} + \frac{\gamma_i - \gamma_{i-1}}{t_i - t_{i-1}}\right) \tag{2}$$

In the equation, γ_{i-1}、γ_{i+1} and γ are the shear strain values at time t_{i-1}, t and t_{i+1}.

According to Equa.(1) and Equa.(2), the apparent viscosity of post-liquefaction Shibei tableland loess is calculated, and the variation curve of apparent viscosity with shear loading time is drawn, as shown in Fig.5. It can be seen from the figure that with the increase of shear loading time, the apparent viscosity of the three samples first increases and

then decreases. In other words, the flow characteristics of the liquefied loess firstly show "shear thickening", and then change to "shear thinning" with the increase of loading time. It can be seen from the figure that confining pressure has a great influence on the fluidity of liquefied loess. The apparent viscosity curve of sby-1 (confining pressure 140 kPa) is more gentle than the other two samples. The possible reason is that the pore water pressure of liquefied loess increases rapidly under low confining pressure, leading to low shear strength and excellent fluidity. The lower the confining pressure is, the smaller the resistance of soil particles is. Therefore, the apparent viscosity of sby-1 is smaller than that of the other two samples.

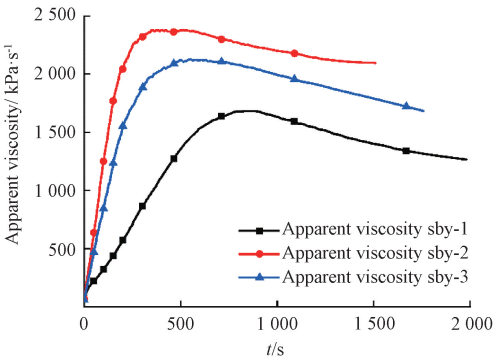

Figure 5 Curves of Apparent viscosity versus time

In order to comprehensively analyze the influence of pore water pressure and effective stress on the apparent viscosity of soil after liquefaction, sby-2 (confining pressure 200 kPa) loess sample is taken as an example. Three curves: Apparent viscosity, pore water pressure, and effective stress against time are drawn (Fig.6). It can be seen from the figure that the pore water pressure of liquefied loess increases nonlinearly under triaxial shear. On the contrary, the effective stress continues to decrease. In particular, the peak time of apparent viscosity is close to the time when pore water pressure and effective stress are equalsuggesting that the increase of apparent viscosity is due to the fact that the loess sample has not reached the state of "complete liquefaction". At this time, the loess sample still has a certain structural strength. In addition, due to the friction between loess particles and the cohesive force produced by the cement among particles, the loess sample still has a large shear strength. With the increase of pore water pressure, the effective stress decreases continuously, and the structure of loess is further destroyed. The partial dissolution of the soluble salt cemented between the particles decreases the cohesion continuously, leading to the continuous decrease of the apparent viscosity. Such result indicates that the fluidity of the Loess is better after liquefaction.

In order to comprehensively analyze the relationship between apparent viscosity and steady-state strength (Yang Zhenmao et al., 2004), sby-1 (confining pressure of 140 kPa) loess sample is selected as an example. The curves of apparent viscosity, deviator stress versus axial strain and pore water pressure with axial strain are drawn (Fig.7 and Fig.8). It can be seen from the figure that with the increase of axial strain, the changing rules of apparent viscosity and deviator stress are similar. When the axial strain is about 8%, both of them reach the peak value at the same time. At this time, with the continuous increase of pore water pressure, the structure of the sample is destroyed rapidly. The resulting

manifestation shows that the strength of the sample decreases rapidly, the axial strain increases rapidly, the apparent viscosity of the sample also decreases, and the fluidity of loess sample tends to be good. When the axial strain is about 18%, the pore water pressure and axial strain gradually reach a stable state, and the change of apparent viscosity is relatively gentle. The results show that the apparent viscosity of the sample will reach a relatively stable value when it reaches the steady state, forming a new flow structure.

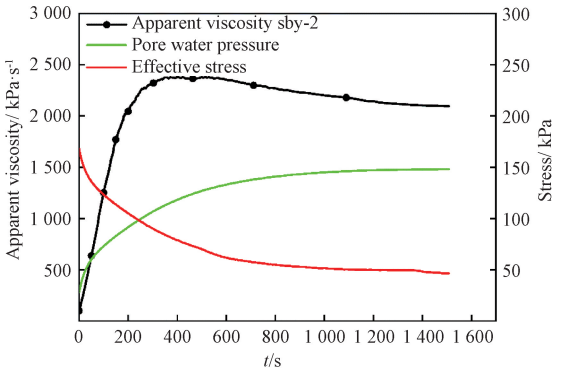

Figure 6 Relationship between Apparent viscosity, Pore water pressure, effective stress and time

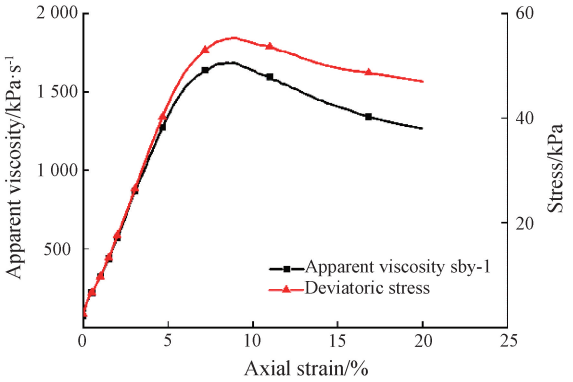

Figure 7 Relationship between Apparent viscosity, Stress and Axial strain

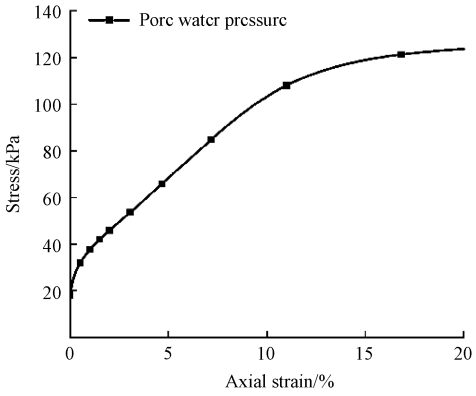

Figure 8 Curves of Pore water pressure versus

3 FORMATION MECHANISM OF LIQUEFACTION FLOW SLIDE DISASTER IN SHIBEI TABLELAND

3.1 Geological Settings of Shibei Tableland Area

In order to better understand the geological environment of Shibei tableland area, the field investigation was carried out in October 2019. In general, the surface of Shibei tableland is a gentle plane with a slope angle less than 3°. The terrain of the entire loess tableland inclines to the northwest, with a higher southeastern part and a lower northwestern part. The overall strike of the flow slide zone is N24°W, with a length of 6 km, a width of 1.2−1.8 km and an area of 9 km^2. The southern boundary of the flow slide zone is shown

in Fig.1. The zone is about 70 km away from the epicenter of the 1920 Haiyuan earthquake, and the seismic intensity is Ⅹ (Wang Lanmin, 2020). The groundwater in the liquefaction flow slide zone is mainly supplied by meteoric water and tableland catchment. The upper phreatic level is 8–20 m (Bai Mingxue et al., 1990). According to the drilling results of 8 boreholes, the stratigraphic distribution of Shibei tableland flow slide area is shown in Fig.9.

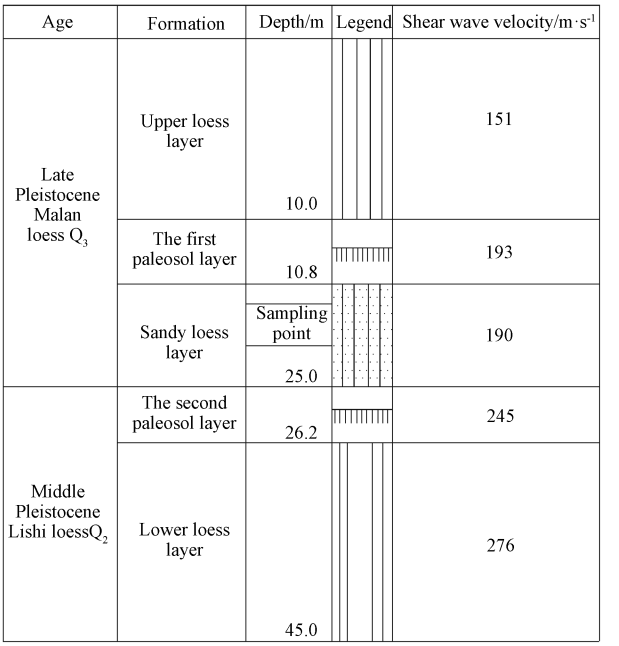

Figure 9 Stratigraphic section of Shibeiyuan area

3.2 Formation Mechanism of Liquefaction Slip Disaster in Shibei Tableland

According to previous studies, before the Haiyuan earthquake, the underground water level in the Shibei tableland had risen abnormally, saturating the loess layer below 10–15 m (Ningxia Hui Autonomous Region Seismological Bureau, 1982; Wang Qian et al., 2014). By referring to Haiyuan seismic data and the recorded description from witnesses, the duration of the main shake in Haiyuan is about 6–15 min (Zhang Xiaochao, 2015). During the calculation process, we assume the duration time is 6 min, refer to the seismic intensity of Shibei tableland area, and consider the site amplification effect of the loose loess strata. Then, in related to the method of equivalence amplitude and action times proposed by Seed, we obtain that the seismic action number is 60, indicating a 60 s duration time and an acceleration of 600 Gal, which correspond to the loading frequency and time of the dynamic triaxial test. The corresponding state of the loess layer is inferred to be "shear thinning". Finally, using unary quadratic function to fit the data of sample sby-1 in the period of "shear thinning", Equa.(3) is obtained:

$$\eta(t) = 10^{-4}t^2 - 0.6754t + 2197.28 \tag{3}$$

$$\tau = \eta\dot{\gamma} \tag{4}$$

$$\frac{1}{2}mv^2 = \tau l \tag{5}$$

Where: m is the mass of the liquefied soil layer, and v is the velocity of the liquefied soil

layer at the end of the earthquake, τ is the internal friction force during the flow of the liquefied soil layer, and l is the flow distance of the liquefied soil layer.

Due to the poor permeability of the paleosol in the upper part of the liquefied soil layer (Wang Lanmin, 2020), the pore water pressure generated in the soil under earthquake can not be dissipated in time. Therefore, the liquefied loess is in the state of "shear thinning". Finally, the apparent viscosity maintains at a relatively stable value. Taking the minimum value of Equa.(3), we can get that $\eta = 1\ 056.8$ kPa/s. According to Seed's method, the number of earthquake actions is 60, the duration is 60 s, the seismic acceleration is 600 Gal, and the converted horizontal acceleration a_x is 0.39 m/s^2 (Wang Lanmin, 2020). According to Equa.(3), (4) and (5), the sliding distance of liquefied soil is 383.79 m, which is consistent with the sliding distance of 300 – 600 m obtained from the field investigation. The seismic force acting on the Loess Tablel and leads to the crack of the upper loess layer, and the liquefied layer is in the "fluid" state, which leads to the alternating action of tension and compression on the liquefied layer and the upper loess layer during sliding. In addition, due to the large pore water pressure in the lower soil mass, once the sagging stress of the overlying strata decreases under the tensile action, the lower soil mass will be ejected upward under the action of pore water pressure. Finally, the landform of alternating peaks and valleys is formed in the flow slide area.

4 CONCLUSION

After reviewing and analyzing previous papers, several seismic cases of large-scale loess liquefaction flow slides induced by earthquake are analyzed. For example, the liquefaction flow slide in Hongdong of Shanxi in 1303 (Zhao Jinquan et al., 2003), the liquefaction flow slide in Dongpu Village caused by Linfen of Shanxi in 1695 (Su Zongzheng et al., 1995), and the liquefaction flow slide in Shibeiyuan Plateau caused by the Haiyuan earthquake in 1920 (Wang Lanmin, 2020). This paper summarizes the common characteristics of large-scale loess liquefaction flow slide induced by earthquake and presents the definition, characteristics and properties of the flow slide phenomenon.

Definition: under the action of earthquake, the phenomenon of large-scale flow slides of contiguous soil with a certain thickness caused by liquefaction in loess sedimentary strata with a surface slope less than 10°. Characteristics and properties: ① The slope angle of the surface is small (less than 10°) when the soil is destroyed, and the collapsed soil is in the state of "flow slide"; ② The length and width of the distribution of the flow slide area are generally from 1km to thousands of meters, and the sliding distance is generally hundreds of meters to more than 1 kilometers; ③ The landform of the flow slide area is interlaced with peaks and valleys; ④ The flow slides are generally induced by strong earthquakes.

Under the action of monotonous shear, the fluidity of the post-liquefaction loess changes from "shear thickening" to "shear thinning" with the increase of duration time, possibly related to the structure of loess. In the process of forming a new stable strength, the apparent viscosity and the variation of the partial stress with axial strain are similar. When the sample reaches the steady state, the apparent viscosity of the sample is also stable.

The forming mechanism of the low-angle liquefaction flow slides in the loess plateau is as follows: Before the earthquake, the rise of groundwater level saturates the sandy loess layers with a depth deeper than 15 m. Then, strong earthquakes rapidly liquefy the saturated

loess layers. Due to the poor water permeability of the ancient soil layers in the upper part of the liquefied soil layers, the pore water pressure in the soil cannot be dissipated in time, resulting in a state of "shear thinning". The seismic force acting on the Loess tableland makes the upper loess layer crack, and the liquefied layer is in the "fluid" state, which results in the alternating action of tension and extrusion on the liquefiable layers and the upper loess layers while sliding. Finally, with the upward action associated with the pore water pressure in the lower soil mass, the interlaced landform of peaks and valleys is generated in the flow slide zone.

REFERENCES

Bai Mingxue, Zhang Sumin. Landslide induced by liquefaction of loessial soil during earthquake of high intensity[J]. *Geotechnical Investigation & Surveying*, 1990(6): 1-5 (in Chinese with English abstract).

Chen Wenhua. Slipping disaster induced by seismic liquefaction [J]. *Journal of Natural Disasters*, 2001, 10(4): 88-93 (in Chinese with English abstract).

Chen Yumin, Liu Hanlong, Shao Guojian, Zhao Nan. Laboratory tests on flow characteristics of liquefied and post-liquefied sand[J]. *Chinese Journal of Geotechnical Engineering*, 2009, 31(9): 1408-1413 (in Chinese with English abstract).

Deng Jin, Wang Lanmin, Wu Zhijian. Establishement and analysis of elasto-plastic loess microstructure and dynamic deformation model[J]. *Chinese Journal of Rock Mechanics and Engineering*, 2013, 32(S2): 3995-4001 (in Chinese with English abstract).

Deng Longsheng, Fan Wen, He Longpeng. Liquefaction property of loess under stochastic seismic load[J]. *Chinese Journal of Rock Mechanics and Engineering*, 2012, 31(6): 1274-1280 (in Chinese with English abstract).

Du Xiuli, Li Yang, Xu Chengshun, Lu Dechun, Xu Zigang, Jin Liu. Review on damage causes and disaster mechanism of Daikai subway station during 1995 Osaka-Kobe earthquake[J]. *Chinese Journal of Geotechnical Engineering*, 2018, 40(2): 223-236 (in Chinese with English abstract).

Hu Zhonghua, Wang Rui, Zhuang Haiyang, Chen Guoxing. Apparent kinetic viscosity of saturated Nanjing sand due to liquefaction-induced large deformation in torsional shear tests [J]. *Chinese Journal of Geotechnical Engineering*, 2016, 38(S2): 149-154 (in Chinese with English abstract).

Huang Yu, Yu Miao, Bhattacharya S. Review on liquefaction-induced damages of soils and foundations during 2011 of the pacific coast of Tohoku earthquake (Japan)[J]. *Chinese Journal of Geotechnical Engineering*, 2013, 35(5): 834-840 (in Chinese with English abstract).

Ishihara K., Okusa S., Oyagi N., Ischuk A. Liquefaction-induced flow slide in the collapsible loess deposit in soviet Tajik[J]. *Soils and Foundations*, 1990, 30(4): 73-89.

Liu Fang, Li Zhen. Probit model for exceedance of liquefaction-induced lateral deformation over a given threshold value due to earthquakes[J]. *Chinese Journal of Geotechnical Engineering*, 2013, 35(S1): 425-429 (in Chinese with English abstract).

Liu Hanlong, Chen Yumin. Analysis of flow characteristics of dynamic torsional tests on post liquefied sand[J]. *Rock and Soil Mechanics*, 2009, 30(6): 1537-1541 (in Chinese with English abstract).

Ningxia Hui Autonomous Region Seismological Bureau. *Catalogue of Ningxia Earthquakes* [M]. Yinchuan: Ningxia People's Press, 1982 (in Chinese).

Prakash S., Puri V. K. Liquefaction of loessial soils [A]. In: Anon. Proc. of Third

International Conference on Sei-smic Mi-crozonation, Seattle, Wash. (Vol Ⅱ) [C]. 1982: 1101-1107.

Puri V.K. Liquefaction behavior and dynamic properties of loessial (Silty) soils[D]. Missouri: University of Missouri-Rolla, 1984.

She Yuexin, Liu Hanlong, Gao Yufeng. Study on liquefaction mechanism and pore-water pressure mode of saturated orginal loess[J]. *Rock and Soil Mechanics*, 2002, 23(4): 395-399 (in Chinese with English abstract).

Su Zongzheng, Shi Zhenliang. Earthquake disaster and relative problems of 1695 Linfen earthquake[J]. *Earthquake Research in Shanxi*, 1995(S1): 150-158 (in Chinese with English abstract).

Wang Lanmin, Liu Hongmei, Li Lan, Sun Chongshao. Laboratory study on the mechanism and beheviors of saturated loess liquefaction [J]. *Chinese Journal of Geotechnical Engineering*, 2000, 22(1): 89-94 (in Chinese with English abstract).

Wang Lanmin, Yuan Zhongxia, Wang Guolie. Study on method for preliminary and detailed evaluation on liquefaction of loess sites[J]. *China Earthquake Engineering Journal*, 2013, 35(1): 1-8 (in Chinese with English abstract).

Wang Lanmin, Liu Yan, Sun Junjie, Tian Wentong, Chai Shaofeng, Xu Shunhua. Shaking-table tests on liquefaction characteristics of saturated undisturbed loess [J]. *China Earthquake Engineering Journal*, 2015, 37(4): 1023-1028 (in Chinese with English abstract).

Wang Lanmin. Mechanism and risk evaluation of sliding flow triggered by liquefaction of loess deposit during earthquakes[J]. *Chinese Journal of Geotechnical Engineering*, 2020, 42(1): 1-19 (in Chinese with English abstract).

Wang Qian, Wang Jun, Wang Lanmin, Wang Ping, Zhong Xiumei. Discussion on mechanism of seismic liquefaction of saturation loess in Shibei Tableland, Guyuan city[J]. *Chinese Journal of Rock Mechanics and Engineering*, 2014, 33(S2): 4168-4173 (in Chinese with English abstract).

Watkinsonim H. R. Impact of communal irrigation on the 2018 Palu earthquake-triggered landslides[J]. *Nature Geoscience*, 2019, 12(11): 940-945.

Wei Xing, Zhang Zhao, Wang Gang, Zhang Jianmin. DEM study of mechanism of large post-liquefaction deformation of saturated sand[J]. *Rock and Soil Mechanics*, 2019, 40(4): 1596-1602, 1625 (in Chinese with English abstract).

Xu Shunhua, Wu Zhijian, Sun Junjie, Yan Wujian, Su Hejun, Su Yongqi. Study of the characteristics and inducing mechanism of typical earthquake landslides of the Minxian-Zhangxian M_S6.6 earthquake[J]. *China Earthquake Engineering Journal*, 2013, 35(3): 471-476 (in Chinese with English abstract).

Yang Zhenmao, Zhao Chenggang, Wang Lanmin, Rao Weiguo. Liquefaction behaviors and steady state strength of saturated loess [J]. *Chinese Journal of Rock Mechanics and Engineering*, 2004, 23(22): 3853-3860 (in Chinese with English abstract).

Zhang Xiaochao. Experimental study on mechanism of Shibeiyuan loess landslide triggered by earthquake[D]. Chengdu: Chengdu University of Technology, 2015 (in Chinese).

Zhang Xiaochao, Pei Xiangjun, Jia Jun, Sun Pingping. Experimental study on the lateral flow slide mechanism of saturated loess mass[J]. *Journal of Geomechanics*, 2018, 24(5): 730-736 (in Chinese with English abstract).

Zhao Jinquan, Zhang Dawei, Gao Shuyi, Su Zongzheng. Huanbu ground slide, the relic of 1303 Hongtong, Shanxi, earthquake of $M8$[J]. *Earthquake Research in Shanxi*, 2003(3): 16-22 (in Chinese with English abstract).

Zhou Zhenglong, Chen Guoxing, Wu Qi. Effect of initial static shear stress on liquefaction and large deformation behaviors of saturated silt[J]. *Rock and Soil Mechanics*, 2017, 38(5): 1314-1320 (in Chinese with English abstract).

Zhuang Haiyang, Hu Zhonghua, Wang Rui, Chen Guoxing. Cyclic torsional shear loading tests on the extremely large post-liquefaction flow deformation of saturated Nanjing sand[J]. *Chinese Journal of Geotechnical Engineering*, 2016, 38(12): 2164-2174 (in Chinese with English abstract).

About the Author

MA Xingyu, born in 1994, is a master degree candidate of Lanzhou Institute of Seismology, China Earthquake Administration. His major research interest is Geotechnical Earthquake Engineering. E-mail: 1748214594@qq.com

Corresponding author: WANG Qian, born in 1985, is an associate researcher in Key Laboratory of Loess Earthquake Engineering, China Earthquake Agency. His major research interest are Soil Dynamics and Geotechnical Earthquake Engineering. E-mail: wangqian@gsdzj.gov.cn